Supporting Information

Optimizing Electrons Donation and Backdonation Effect by A Combination of d-Block Transition Metal and s-Block Calcium Atoms for Efficient Nitrogen Fixation

Lingli Liu,[a] Guanping Wei,[a] Zongchang Mao,[a] Tiantian Hao,[a] Ling Zhu,[a] Xijun Wang,[c] and Shaobin Tang[a,b*]*

[a]Jiangxi Provincial Key Laboratory of Synthetic Pharmaceutical Chemistry, Gannan Normal University, Ganzhou 341000, China

[b]Engineering Research Center of Bamboo Advanced Materials and Conversion of Jiangxi Province, Gannan Normal University, Ganzhou 341000, China

[c] Department of Chemical and Biological Engineering, Northwestern University, 2145 Sheridan Road, Evanston, Illinois 60208, United States.

Authors to whom all correspondence should be addressed:

*Email: zhuling05@gnnu.edu.cn

tsb1980@xmu.edu.cn

Table S1. The adsorption energy of N_2 (in eV)) on TM-Ca DACs catalysts with different supercell size.

catalyst	5 × 5	6 × 6	7 × 7
Sc-Ca	-1.18	-1.17	-1.12
Ti-Ca	-1.57	-1.58	-1.58
V-Ca	-1.45	-1.46	-1.45
Cr-Ca	-0.76	-0.69	-0.70
Mn-Ca	-0.74	-0.75	-0.76
Mo-Ca	-1.89	-1.83	-1.86

Table S2. The adsorption energy of N_2 (in eV) on TM-Ca DACs catalysts with different k-point sampling.

catalyst	3 × 3 × 1	4 × 4 × 1	5 × 5 × 1	6 × 6 × 1
Sc-Ca	-1.17	-1.15	-1.15	-1.15
Ti-Ca	-1.58	-1.58	-1.58	-1.57
Cr-Ca	-0.69	-0.69	-0.69	-0.69

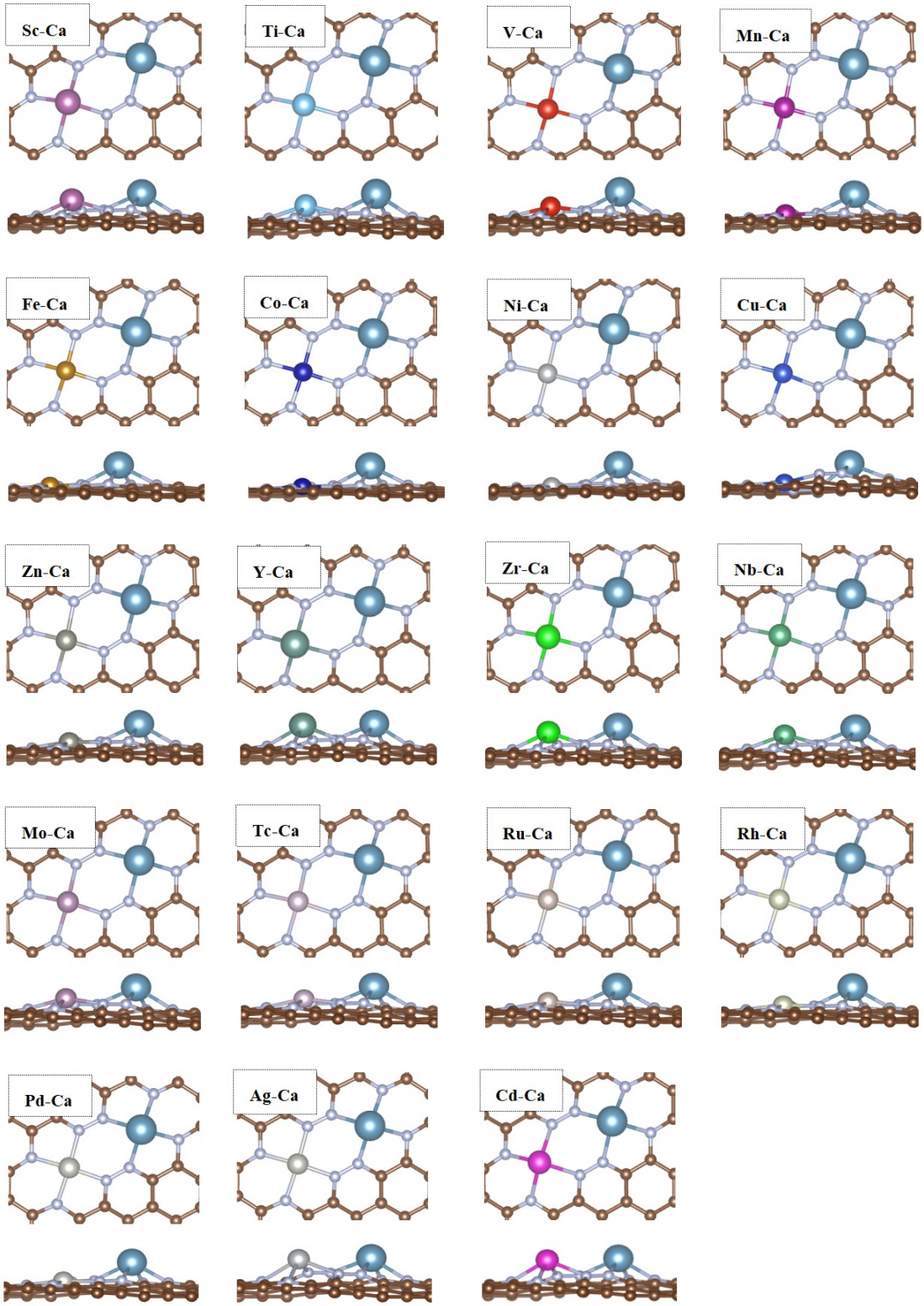

Fig. S1. Top and side view of optimized geometrical structures of TM-Ca DACs.

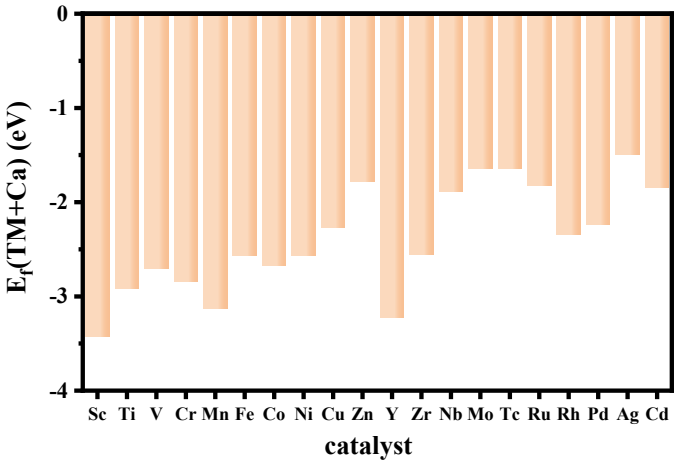

Fig. S2. The calculated formation energy of TM-Ca pair per atom.

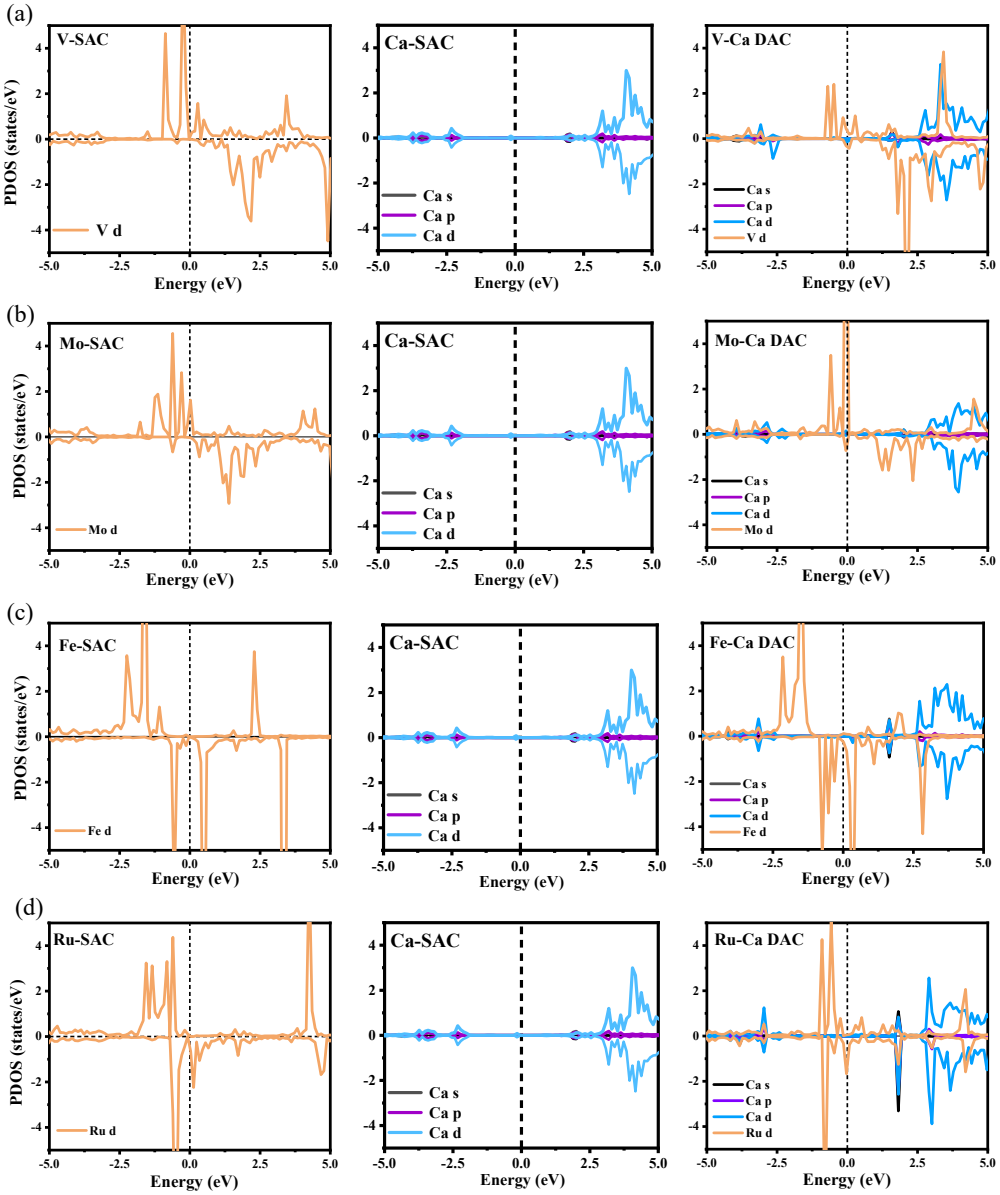

Fig. S3. Spin-polarized PDOS of the d orbitals of TM and s, p and d orbitals of Ca atoms of TM-Ca pair and corresponding single atom: (a) TM = V, (b) Mo, (c) Fe, and Ru. The Fermi level is set to 0.

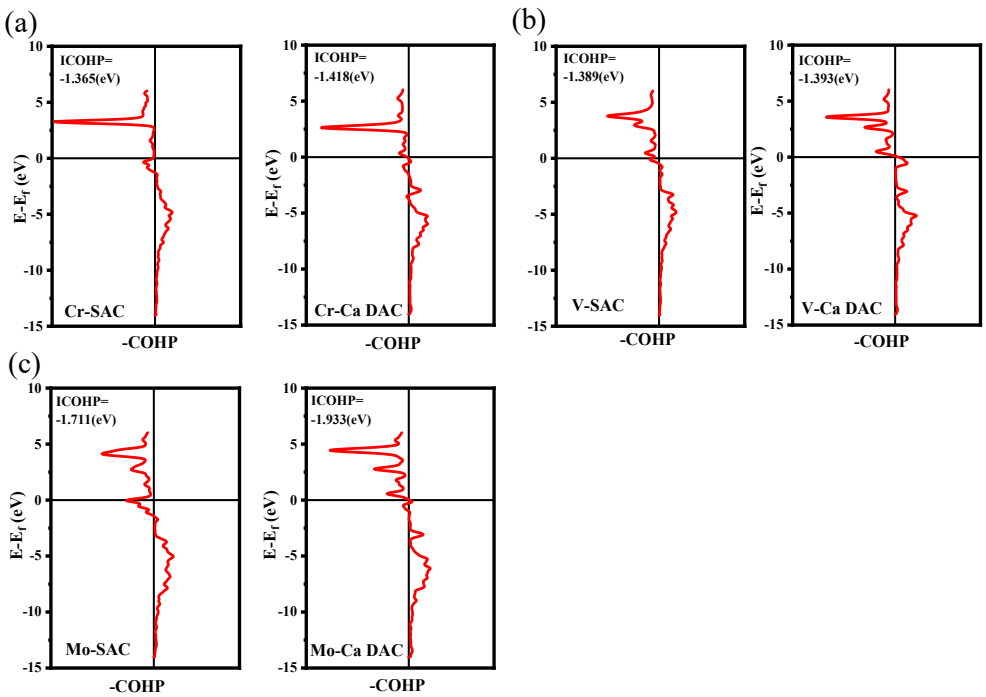

Fig. S4. The calculated COHP of the TM—N coordination bond on TM SAC and TM-Ca DACs: (a) TM = Cr, (b) V, and (c) Mo.

Table S3. Adsorption energy (in eV) of different types of intermediates $*N_2$ on TM-Ca DACs for NRR**,** including side-on/ end-on and side-on-TM/ end-on-TM. (The horizontal line indicates that this adsorption configuration does not exist).

catalysts	side-on	end-on	end-on-TM	side-on-TM
Sc-Ca	-1.17	——	-0.97	——
Ti-Ca	-1.58	——	-1.41	——
V-Ca	-1.46	——	——	-0.92
Cr-Ca	-0.69	——	-0.64	——
Mn-Ca	-0.75	——	——	0.03
Fe-Ca	-0.79	——	-0.82	-0.12
Co-Ca	-0.44	——	-0.25	——
Ni-Ca	-0.41	——	——	——
Cu-Ca	-0.04	——	——	——
Zn-Ca	-0.41	——	——	——
Y-Ca	-1.05	——	-0.83	——
Zr-Ca	-1.56	——	——	——
Nb-Ca	-1.85	——	——	——
Mo-Ca	-1.83	——	——	-1.24
Tc-Ca	-1.65	——	——	-0.85
Ru-Ca	-0.93	-0.35	-0.91	-0.36
Rh-Ca	-0.41	——	——	——
Pd-Ca	-0.36	——	——	——
Ag-Ca	-0.56	——	-0.42	——
Cd-Ca	-0.55	0.36	——	——

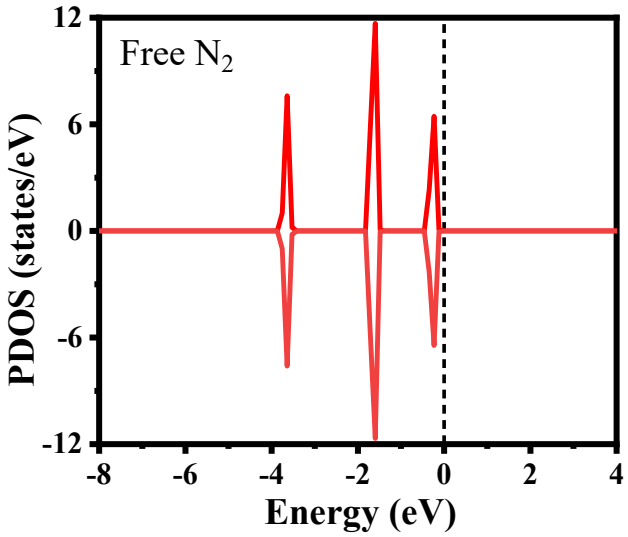

Fig. S5. The density of states (DOS) of free N_2.

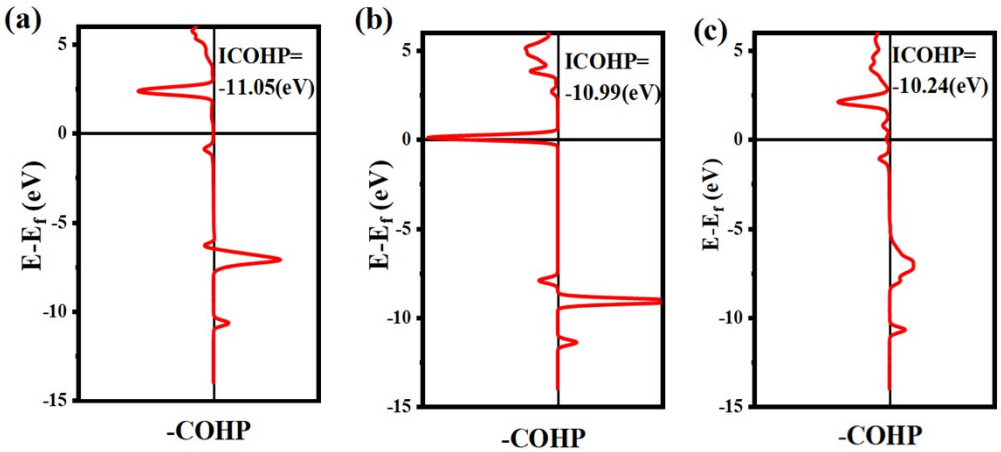

Fig. S6. The COHP of the N≡ N bond for N_2 adsorbed on (a) Cr SAC, (b) Ca SAC, (c) Cr-Ca DAC.

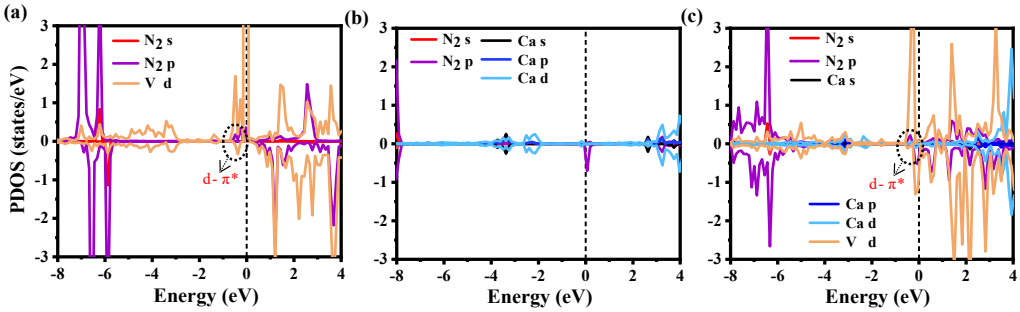

Fig. S7. Spin polarized PDOS of the d orbitals of V, s, p and d orbitals of Ca, and s and p orbitals of *N_2 for N_2 adsorbed on (a) V SAC, (b) Ca SAC, (c) V-Ca DAC.

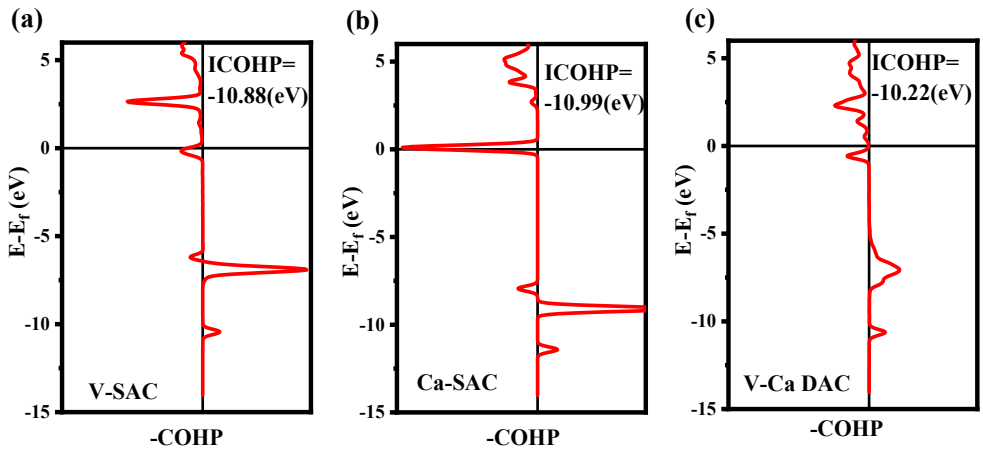

Fig. S8. The COHP of the N≡ N bond for N_2 adsorbed on (a) V SAC, (b) Ca SAC, (c) V-Ca DAC.

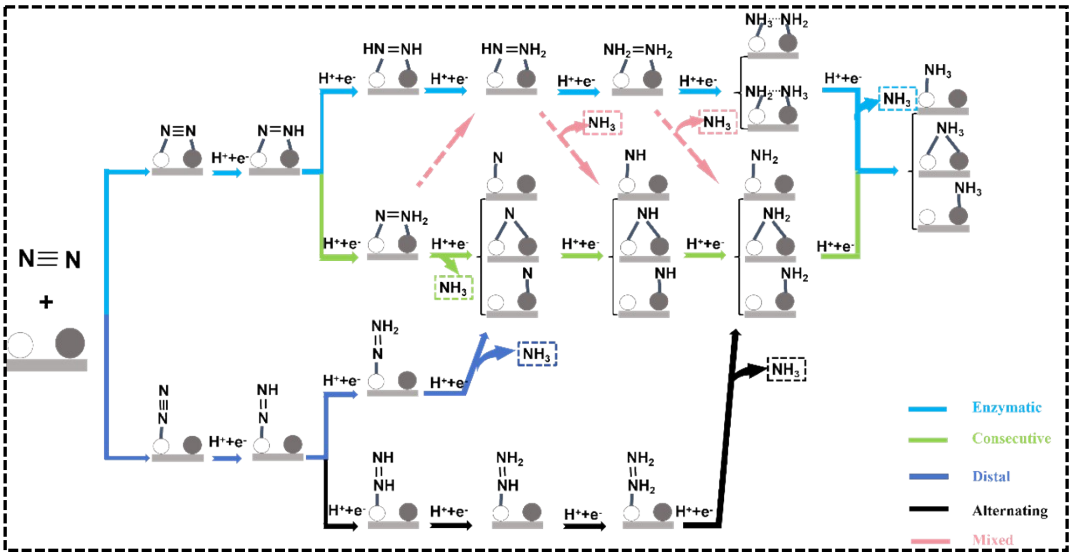

Fig. S9. Schematic illustration for possible eNRR pathways on TM-Ca DACs.

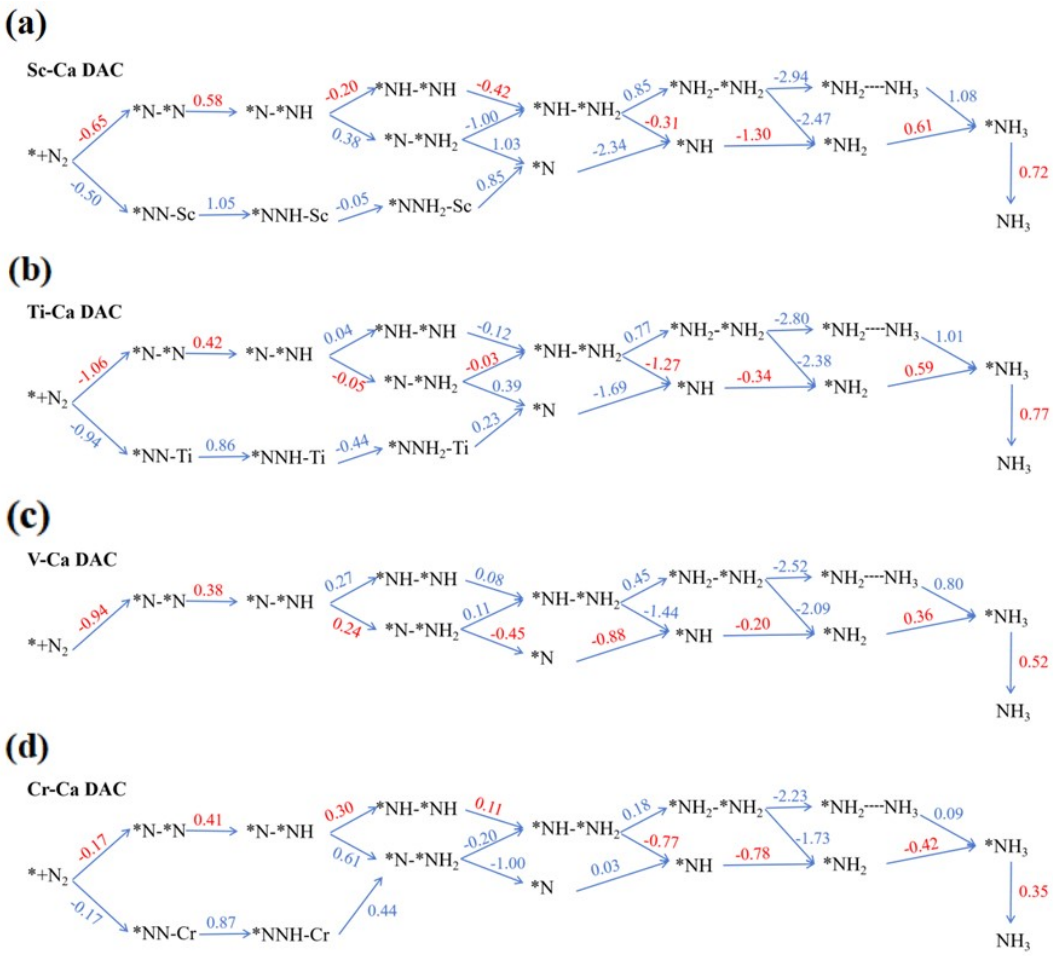

Fig. S10. Underlying reaction pathways of N_2 reduction to NH_3 on the TM-Ca DACs with TM = (a) Sc, (b) Ti, (c) V, and (d) Cr and free energy change (in eV) of each elementary step, with the optimal pathway indicated in red.

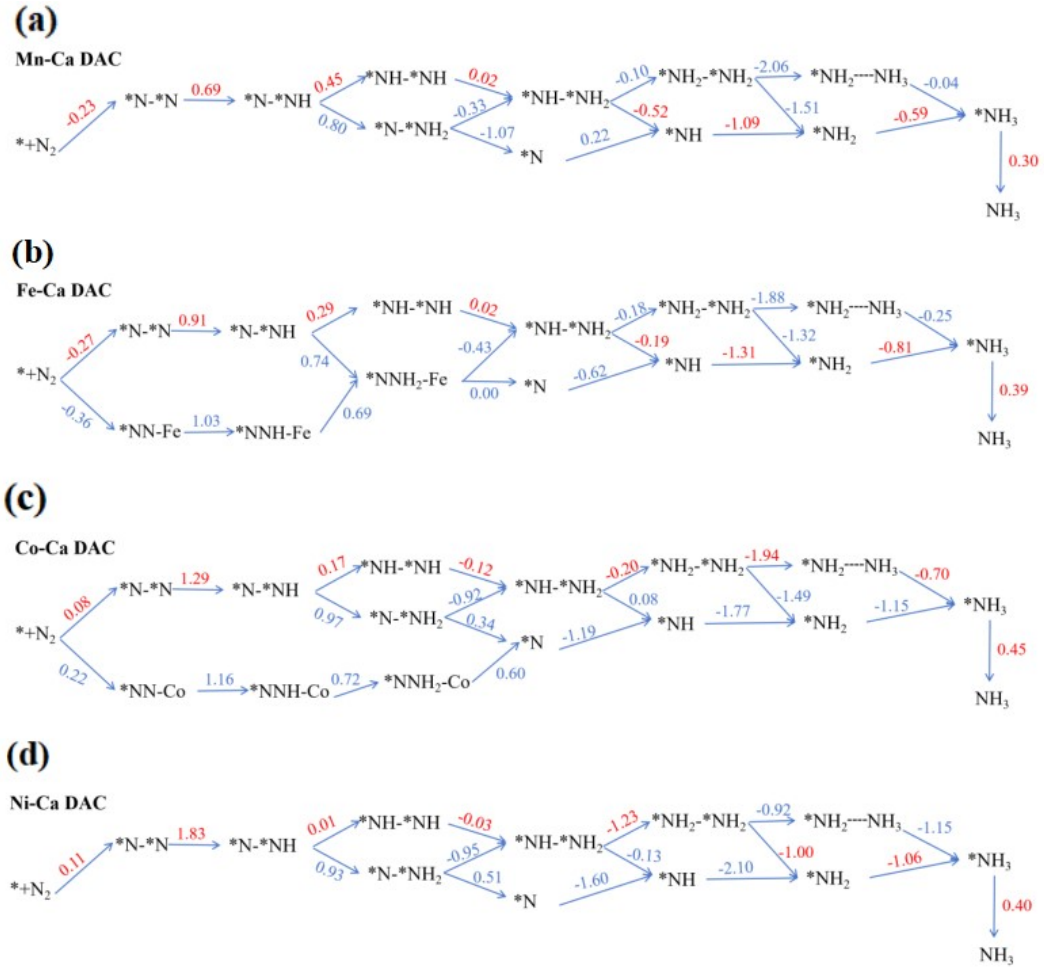

Fig. S11. Underlying reaction pathways of N_2 reduction to NH_3 on the TM-Ca DACs with TM = (a) Mn, (b) Fe, (c) Co, and (d) Ni and corresponding free energy change (in eV) of each elementary step, with the optimal pathway indicated in red.

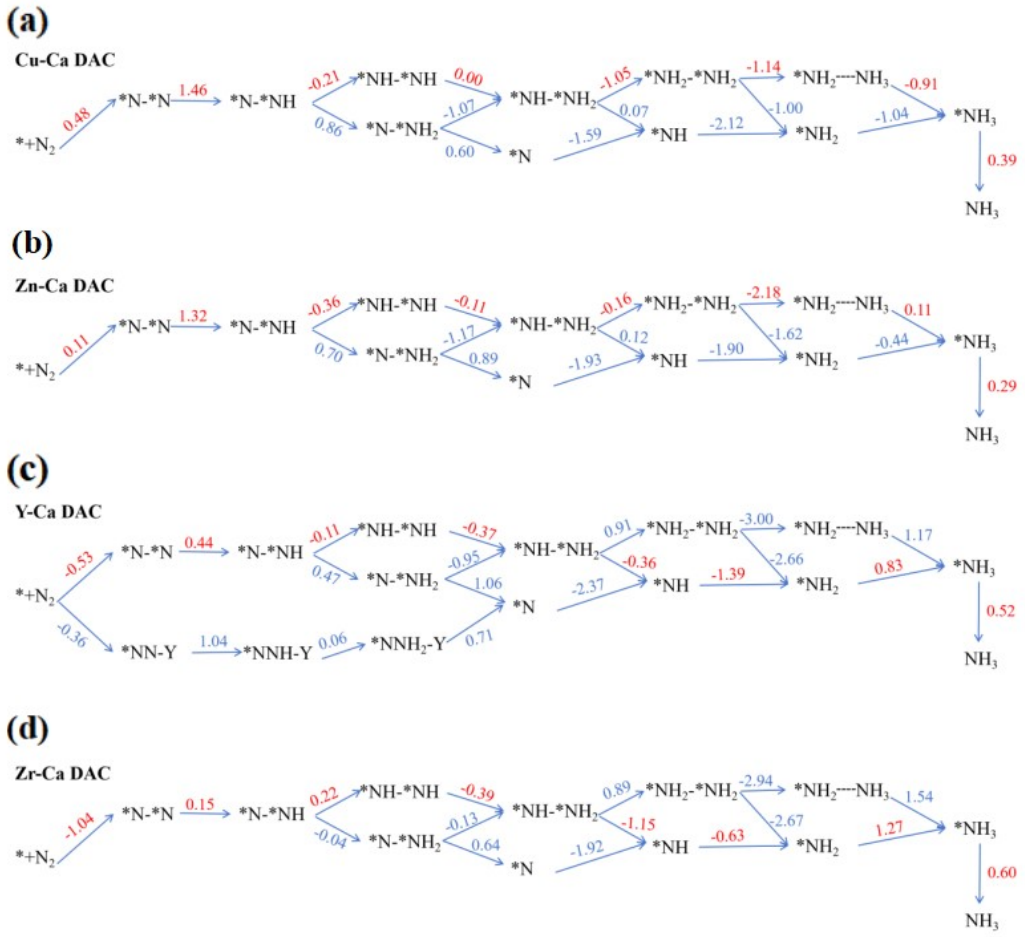

Fig. S12. Underlying reaction pathways of N_2 reduction to NH_3 on the TM-Ca DACs with TM = (a) Cu, (b) Zn, (c) Y, and (d) Zr and corresponding free energy change (in eV) of each elementary step, with the optimal pathway indicated in red.

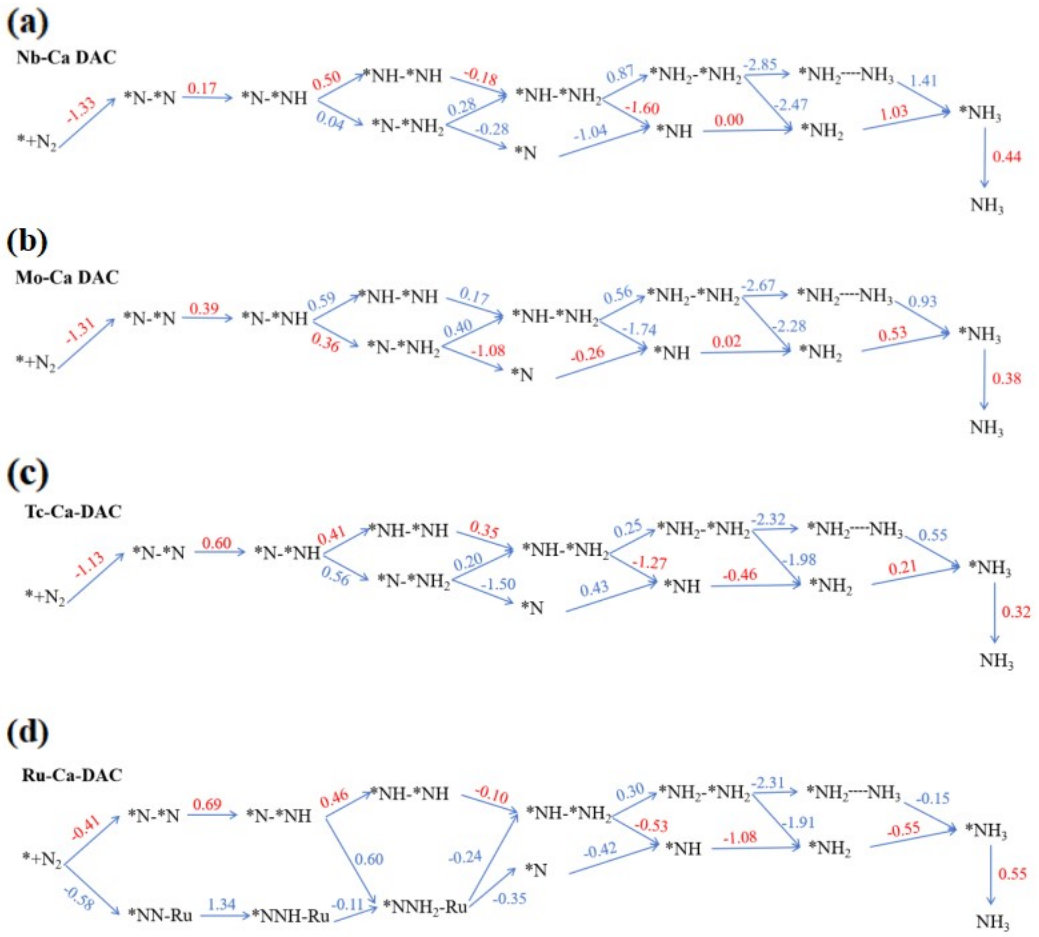

Fig. S13. Underlying reaction pathways of N_2 reduction to NH_3 on the TM-Ca DACs with TM = (a) Nb, (b) Mo, (c) Tc, and (d) Ru and corresponding free energy change (in eV) of each elementary step, with the optimal pathway indicated in red.

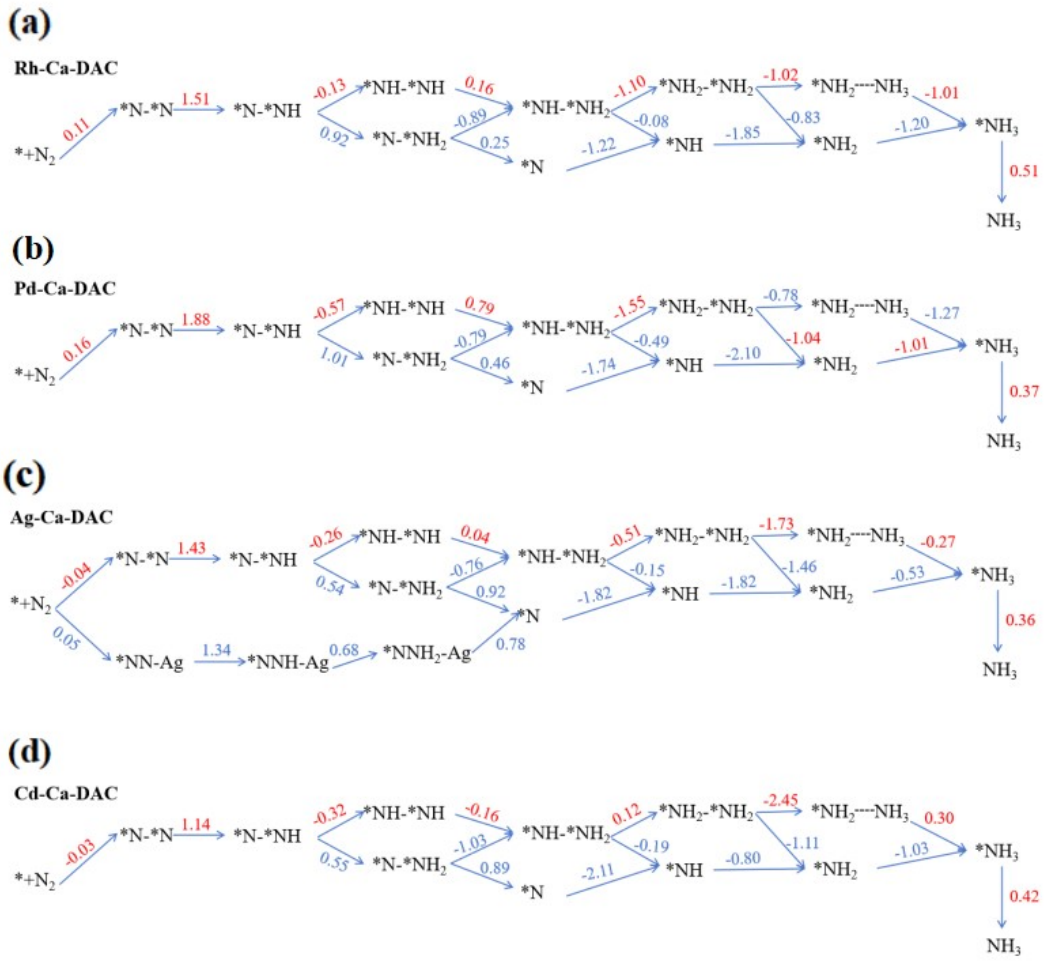

Fig. S14. Underlying reaction pathways of N_2 reduction to NH_3 on the TM-Ca DACs with TM = (a) Rh, (b) Pd, (c) Ag, and (d) Cd and corresponding free energy change (in eV) of each elementary step, with the optimal pathway indicated in red.

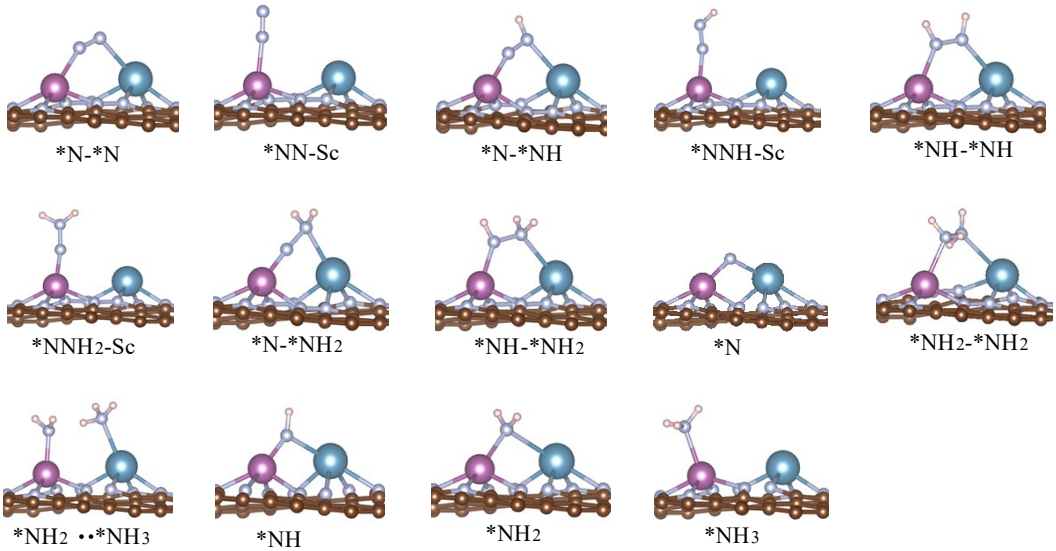

Fig. S15. Optimized structures of NRR reaction intermediates on TM-Ca DACs.

Table S4. Free energy corrections. Computed zero-point energies (ZPE) and entropies multiplied by T (T = 298.15 k) (-TS) for adsorbed species.

TM-Ca DACs			
Species	E_{ZPE} **(eV)**	***TS* (eV)**	E_{ZPE} **-*TS* (eV)**
Enzymatic			
*N-*N	0.201	0.126	0.075
*N-*NH	0.500	0.111	0.389
*NH-*NH	0.816	0.132	0.684
NH-NH_2	1.142	0.164	0.978
NH_2-NH_2	1.501	0.202	1.299
*NH_2···NH_3	1.667	0.255	1.412
*NH_3	1.006	0.208	0.798
Consecutive			
*N-*N	0.201	0.126	0.075
*N-*NH	0.500	0.111	0.389
N-NH_2	0.815	0.149	0.666
*N	0.087	0.056	0.031
*NH	0.336	0.102	0.234
*NH_2	0.674	0.098	0.576
*NH_3	1.006	0.208	0.798
Distal			
*NN-TM	0.200	0.177	0.023
*NNH-TM	0.475	0.169	0.306
*NNH_2-TM	0.772	0.203	0.569
TM SACs			
*N_2	0.254	0.084	0.170
*NNH	0.498	0.108	0.390
*NHNH	0.799	0.208	0.591
*$NHNH_2$	1.115	0.225	0.890
*NH	0.330	0.090	0.240
*NH_2	0.707	0.080	0.627
*NH_3	1.091	0.097	0.994
*NNH_2	0.813	0.178	0.635
*N	0.086	0.061	0.025

Table S5. Free energy changes (in eV) of all elementary steps along the favorable reaction pathway by TM-Ca DACs. Numbers in blue indicate the maximum free energy barrier among all elementary steps.

catalysts	*→ *N-*N	*N-*N→ *N-*NH	*N-*NH→ *NH-*NH	*NH-*NH→ *NH-*NH_2	*NH-*NH_2→ *NH	*NH→ *NH_2	*NH_2→ *NH_3	*NH_3→ *
Sc-Ca	-0.65	0.58	-0.20	-0.42	-0.31	-1.30	0.61	0.72
Cr-Ca	-0.17	0.41	0.30	0.11	-0.77	-0.78	-0.42	0.35
Mn-Ca	-0.23	0.69	0.45	0.02	-0.52	-1.09	-0.59	0.30
Fe-Ca	-0.27	0.91	0.29	0.02	-0.19	-1.31	-0.81	0.39
Y-Ca	-0.53	0.44	-0.11	-0.37	-0.36	-1.39	0.83	0.52
Zr-Ca	-1.04	0.15	0.22	-0.39	-1.15	-0.63	1.27	0.60
Nb-Ca	-1.33	0.17	0.50	-0.18	-1.60	0.00	1.03	0.44
Tc-Ca	-1.13	0.60	0.41	0.35	-1.27	-0.46	0.21	0.32
Ru-Ca	-0.41	0.69	0.46	-0.10	-0.53	-1.08	-0.55	0.55
	*→ *N-*N	*N-*N→ *N-*NH	*N-*NH→ *N-*NH_2	*N-*NH_2→ *N	*N→ *NH	*NH→ *NH_2	*NH_2→ *NH_3	*NH_3→ *
V-Ca	-0.94	0.38	0.24	-0.45	-0.88	-0.20	0.37	0.51
Mo-Ca	-1.31	0.39	0.36	-1.08	-0.26	0.02	0.53	0.38
	*→ *N-*N	*N-*N→ *N-*NH	*N-*NH→ *N-*NH_2	*N-*NH_2→ *NH-*NH_2	*NH-*NH_2→ *NH	*NH→ *NH_2	*NH_2→ *NH_3	*NH_3→ *
Ti-Ca	-1.06	0.42	-0.05	-0.03	-1.27	-0.34	0.59	0.77
	*→ *N-*N	*N-*N→ *N-*NH	*N-*NH→ *NH-*NH	*NH-*NH→ *NH-*NH_2	*NH-*NH_2→ *NH_2-*NH_2	*NH_2-*NH_2→ *NH_2···*NH_3	*NH_2···*NH_3→ *NH_3	*NH_3→ *
Co-Ca	0.08	1.29	0.17	-0.12	-0.20	-1.94	-0.70	0.45
Cu-Ca	0.48	1.46	-0.21	0.00	-1.05	-1.14	-0.91	0.39
Zn-Ca	0.11	1.32	-0.36	-0.11	-0.16	-2.18	0.11	0.29
Rh-Ca	0.11	1.51	-0.13	0.16	-1.10	-1.02	-1.01	0.51
Ag-Ca	-0.04	1.43	-0.26	0.04	-0.51	-1.73	-0.27	0.36
	*→ *N-*N	*N-*N→ *N-*NH	*N-*NH→ *NH-*NH	*NH-*NH→ *NH-*NH_2	*NH-*NH_2→ *NH_2-*NH_2	*NH_2-*NH_2→ *NH_2	*NH_2→ *NH_3	*NH_3→ *
Ni-Ca	0.11	1.83	0.01	-0.03	-1.23	-1.00	-1.06	0.40
Pd-Ca	0.16	1.88	-0.57	0.79	-1.55	-1.04	-1.01	0.37

Table S6. Comparison of results from promising TM-Ca DACs and previously reported eNRR electrocatalysts. Limiting potential (U_L in V).

Substrate	Active site	U_L	References
G	**V-Ca**	**-0.38**	**This work**
G	**Cr-Ca**	**-0.41**	**This work**
G	Ca	-0.67	Ref.1
C_3N_4	B	-0.47	Ref.2
C_2N	Mo	-0.53	Ref.3
G	Mo	-0.99	Ref.4
Pc	V_2	-0.39	Ref.5
TMD	CaBa-$MoSe_2$	-0.60	Ref.6
BNNT	Ti	-0.36	Ref.7

Table S7. The adsorption energy of N_xH_y (ΔE ($*N_xH_y$), in eV)) on Cr-SAC and Cr-Ca DACs catalysts.

ΔE ($*N_xH_y$)	**Cr-SAC**	**Cr-Ca DAC**
$*N_2$	-0.46	-0.69
*NNH	-0.13	-0.66
*NHNH	-0.08	-0.81
$*NHNH_2$	-0.56	-0.97
*NH	-0.17	-0.16
$*NH_2$	-1.19	-1.34
$*NH_3$	-1.75	-2.05

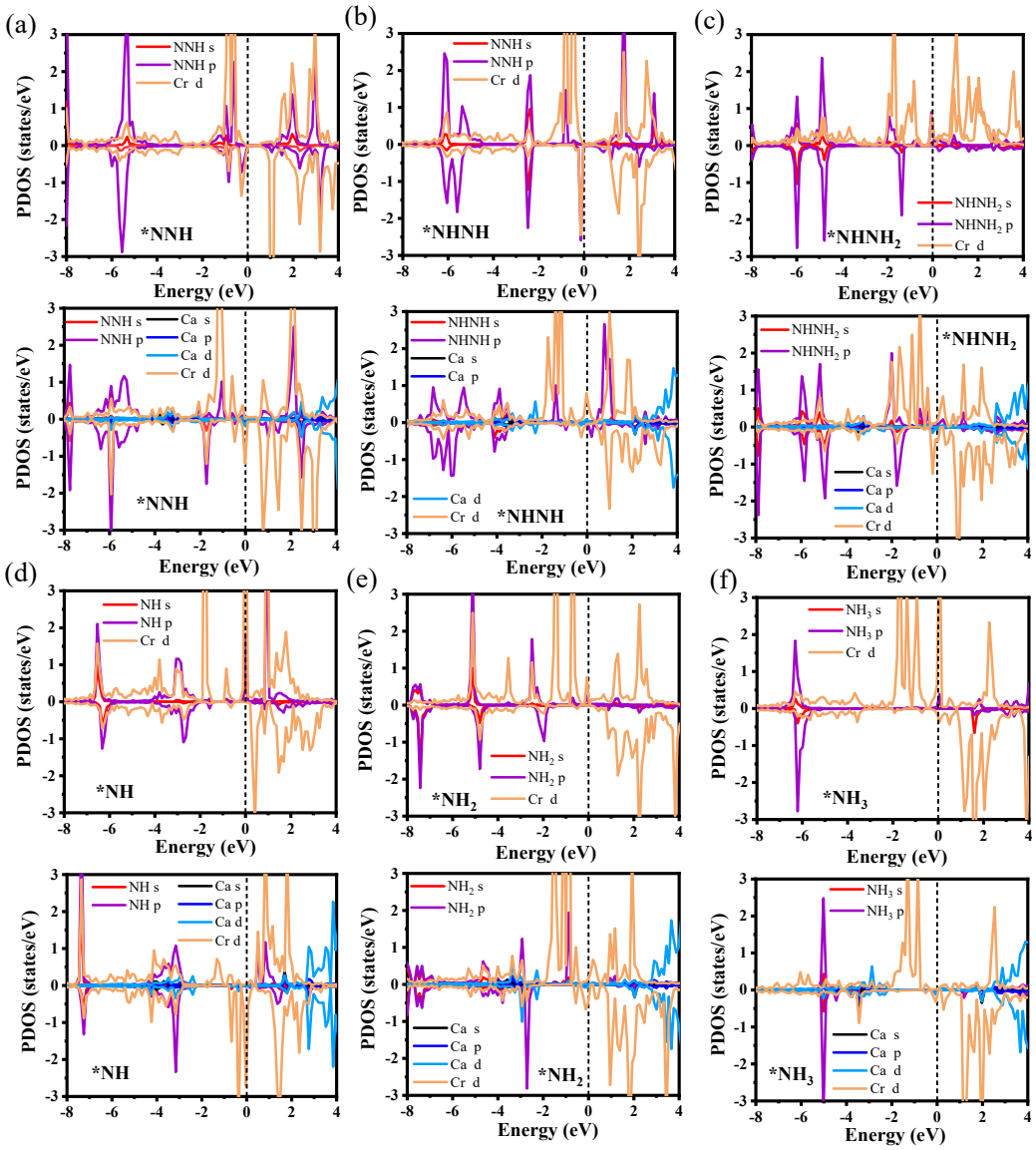

Fig. S16. Spin-polarized PDOS of the d orbitals of Cr, s, p and d orbitals of Ca, and s and p orbitals of N_xH_y intermediates adsorbed on Cr SAC (top panel) and Cr-Ca DAC (bottom panel). The Fermi level is set to 0.

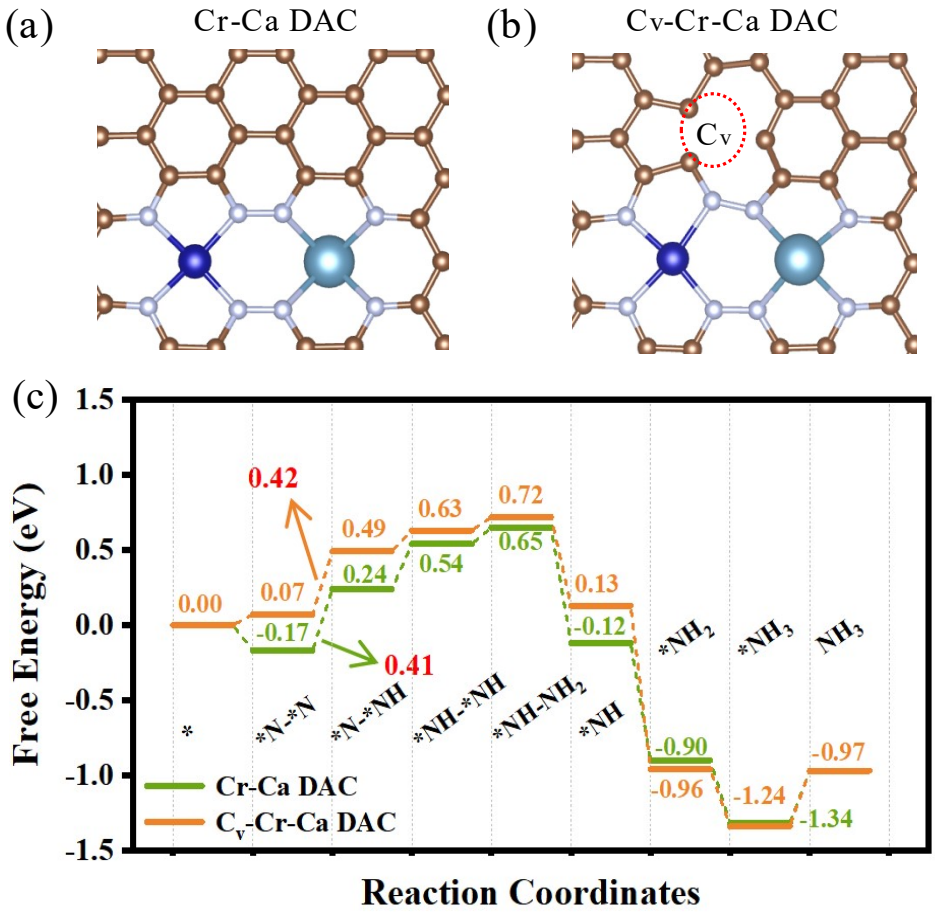

Fig. S17. A comparison of (a) geometry structure of Cr-Ca pair with and without carbon vacancy defect and (b) free energy diagram of eNRR catalyzed by these catalysts. The arrows define the free energy change of PDS.

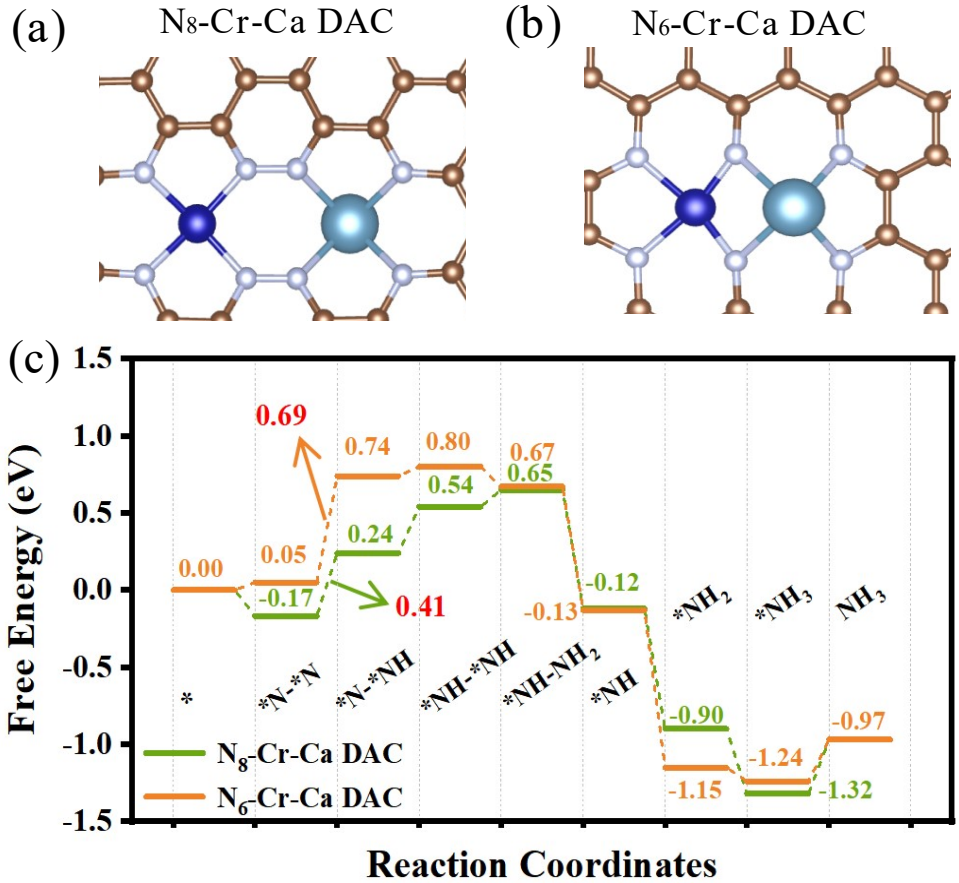

Fig. S18. A comparison of geometry structure and free energy diagram of NRR for the Cr-Ca pair with N_8V_4 and N_6 coordination structures. The arrows define the free energy change of PDS.

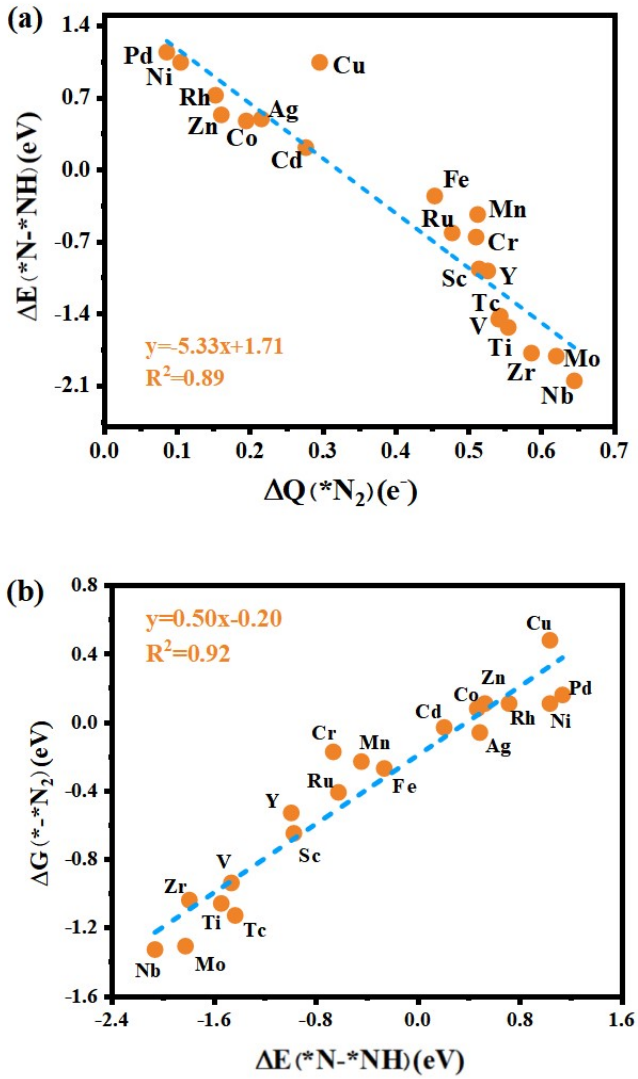

Fig. S19. The relationship between the ΔE(*N-*NH) and (a) the polarized charge of N_2 (ΔQ(*N_2)), and (b) adsorption energy of *N_2 (ΔG(*N_2).

References

1 T. Liu, X. Qu, Y. Zhang, X. Wang, Q. Dang, X. Li, B. Wang, S. Tang, Y. Luo and J. Jiang, Regulating the charge densities of s-block calcium single-atom site catalysts for efficient N_2 activation and reduction, *Chem. Eng. J.*, 2023, **457**,141187.

2 C. Ling, X. Niu, Q. Li, A. Du and J. Wang, Metal-free single atom catalyst for N_2 fixation driven by visible light, *J. Am. Chem. Soc.*, 2018, **140**, 14161-14168.

3 Z. Wang, Z. Yu and J. Zhao, Computational screening of a single transition metal atom supported on the C_2N monolayer for electrochemical ammonia synthesis, *Phys. Chem. Chem. Phys.*, 2018, **20**, 12835-12844.

4 L. Hui, Y. Xue, H. Yu, Y. Liu, Y. Fang, C. Xing, B. Huang and Y. Li, Highly efficient and selective generation of ammonia and hydrogen on a graphdiyne-based catalyst, *J. Am. Chem. Soc.*, 2019, **141**, 10677-10683.

5 X. Guo, J. Gu, S. Lin, S. Zhang, Z. Chen and S. Huang, Highly efficient and selective generation of ammonia and hydrogen on a graphdiyne-based catalyst, *J. Am. Chem. Soc.*, 2020, **142**, 5709-5721.

6 D. Wu, J. Wu, H. Li, W. Lv, Y. Song, D. Ma and Y. Jia, Unlocking the potential of alkaline-earth metal active centers for nitrogen activation and ammonia synthesis: the role of s–d orbital synergy, *J. Mater. Chem. A*, 2024, **12**, 4278-4289.

7 S. Zhou, X. Yang, X. Xu, S. X. Dou, Y. Du and J. Zhao, Boron nitride nanotubes for ammonia synthesis: activation by filling transition metals, *J. Am. Chem. Soc.*, 2020, **142**, 308-317.